Revista Mexicana de Física **39**, *Suplemento 2 (1993) 21-28*

Some new aspects of nuclear structure near the drip lines

B. ALEX BROWN
National Superconducting Cyclotron Laboratory
and
Department of Physics and Astronomy
Michigan State University, East Lansing, Michigan 48824, USA

ABSTRACT. Large-scale shell-model calculations are used to extrapolate nuclear binding energies to the neutron drip line in light nuclei. The special features associated with the major-oscillator shell inversion (intruder states) in the regions of ^{12}Be and ^{32}Mg are pointed out.

RESUMEN. Se usan cálculos a gran escala con el modelo de capas para extrapolar las energías de ligadora en iones ligeros ricos en neutrones cerca del límite de estabilidad. Se señalan también casos especiales asociados con inversiones de las capas de oscilador armónico (estados intrusos) en la región del ^{12}Be y del ^{32}Mg.

PACS: 21.60.Cs; 21.10.Dr

1. INTRODUCTION

One of the great thrusts of experimental and theoretical nuclear structure physics in the 1990's is the exploration of nuclei far from stability, in particular, for light nuclei where the drip lines can most easily be reached experimentally and where large-scale shell-model calculations can be carried out. As one reaches the drip line, new structure phenomena are expected to be observed which will put new and more stringent tests on the nuclear models. I will focus in this paper on the large-scale shell-model interpretation of: (1) the binding energies as one approached the neutron drip line, and (2) major-oscillator shell inversion (intruder states) in the region of ^{32}Mg. There are many other topics of interest which I will not be able to cover in this paper. Among these for nuclei near the proton drip line are the Gamow-Teller beta decay strength distributions [1], beta-delayed particle decay [2], direct diproton decay [3], and proton halos has they show up in the quadrupole moments [4,5]. Near the neutron drip line and especially in ^{11}Li there is at present much interest in the interpretation of neutron halos and the associated soft-dipole mode of excitation [6,7].

Modern shell-model calculations incorporate as many of the important configurations as possible and make use of realistic effective interactions for the valence nucleons [8]. With the OXBASH shell-model code [9] run on VAX computers, treatment of cases with J-scheme dimensions of up to about 7,000 is routine [10]. At this level of complexity one is able to consider the full basis for both protons and neutrons in the $0p$ or $1s0d$ major shells, as well as for protons in the $0p$ shell combined with neutrons in the $1s0d$ shell. For many cases in which protons in the $1s0d$ shell are combined with neutrons in the $1p0f$ shell, the

TABLE I. Table of model spaces and interactions.

Model space	Interaction	Type	Code[a]	Reference
$0p$ (p)	Cohen-Kurath	TBME	CK	[14]
	Warburton-Brown	TBME	WB	[15]
$1s0d$ (sd)	Wildenthal	TBME + G	W	[16]
	Brown *et al.*	POT	SDPOTA	[17]
$1p0f$ (pf)	McGrory	TBME + G	MG	[18]
	Richter *et al.*	TBME + G	FPMI3	[19]
	Richter *et al.*	POT	FPD6	[19]
	Nakada *et al.*	G	FPRKB	[13]
p–sd	Warburton-Brown	POT	WB	[15]
	Millener-Kurath	POT	MK	[20]
sd–pf	Warburton *et al.*	POT	WBMB	[11]

[a]Shorthand name for the interaction used in OXBASH [9] and in the discussion.

dimensions are already over 7000. However, many interesting sd–pf studies are possible, and we have considered a few cases in the sd–pf model space with J-scheme dimensions up to about 12,000 [11]. Larger dimensions can be considered with other codes designed to run on supercomputers [12,13].

Model spaces and interactions used in recent calculations are summarized in Table I. I give the interactions used within the major shells (p, sd and pf) and the cross-shell interaction for the combined shells (p–sd and sd–pf). The total interaction in the combined shells is composed of three parts representing the components within the two major shell plus the cross terms. All interactions have been adjusted by a least-squares fit to some selection of binding energy and excitation energy data. This was accomplished by varying individual two-body matrix elements (TBME), by varying well determined linear combinations of two-body matrix elements and keeping the rest fixed at some G matrix values (TBME+G), by varying parameters of some potential (POT), or by varying Talmi integrals (TI). These effective interactions are very close to that expected from microscopic G-matrix calculations based on the nucleon-nucleon interaction, but the small differences from the G matrix are very important for detailed spectroscopy [8,10].

Several special properties of the nuclei near the drip lines will now be addressed. First, the binding energy systematics of neutron rich nuclei are discussed in the framework of $0\hbar\omega$ shell-model configurations. "$0\hbar\omega$" means that the nucleons are assumed to fill the lowest available major-oscillator shell configurations. The deviation between experiment and theory in this context for nuclei around ^{32}Mg will then be addressed in terms of cross-shell ($n\hbar\omega$) excitations.

2. BINDING ENERGIES

The first property usually measured for the most exotic nuclei is whether or not they are bound to nucleon decay. When a nucleus is bound to nucleon decay it can only decay

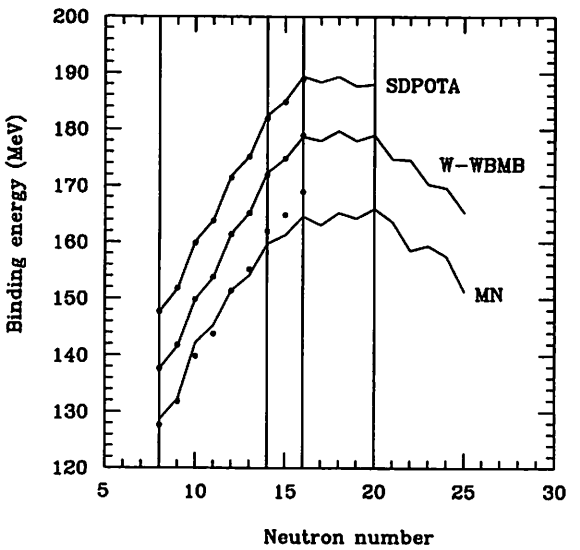

FIGURE 1. Binding energies of the $Z = 8$ isotopes.

by the weak interaction and will have a half-life on the order of milliseconds or greater. This will be referred to as a "stable" nucleus in the discussion below. A nucleus which does decay by nucleon emission will be referred to as "unstable". If a nucleus is stable its mass excess can be measured. Even for unstable nuclei, the mass excess of the ground and excited states can be measured by transfer reactions if the appropriate target is available. The only important nucleon-decay channel for the ground states of unstable neutron-rich nuclei is neutron emission.

There has been excitement recently about the instability of ^{26}O [21]. I show in Fig. 1 binding energy curves for the $Z = 8$ isotopes. The experimental data (circles) are compared with three predictions: the global predictions of Moeller and Nix [22] (MN), the W–*sd* calculation up to $N = 20$ plus the WBMB *sd*–*pf* calculation beyond $N = 20$, and the SDPOTA–*sd* calculation. (For the purpose of display 10 MeV has been added to the W comparison and 20 MeV has been added to the A comparison.)

The shell-model predictions are clearly much better than the global-model predictions in this case. The average deviation between the shell-model predictions and experiment is consistent with the average 180 keV rms deviation found for 447 ground and excited states over the entire sd shell [8,16]. The global model of Moeller and Nix as well as most other global models [23] predict that ^{26}O is stable in contradiction to experiment. However, this is not too surprising, given the rather poor agreement for the other O isotopes. It is more surprising that the W–*sd* calculations also predicts that ^{26}O is stable by about 1 MeV. However, the SDPOTA–*sd* calculation predicts ^{26}O to be unstable, but only by 20 keV. This difference is an indication of the rather large model dependence which can exist in the shell-model extrapolations to exotic nuclei. With both W and SDPOTA ^{27}O and ^{28}O are predicted to be unstable. I now discuss some aspects of the model dependence.

The trend of the $Z = 8$ binding energies can be understood in the extreme j–j coupling limit. I show in Fig. 2 the effective neutron single-particle energy (ESPE) as a function

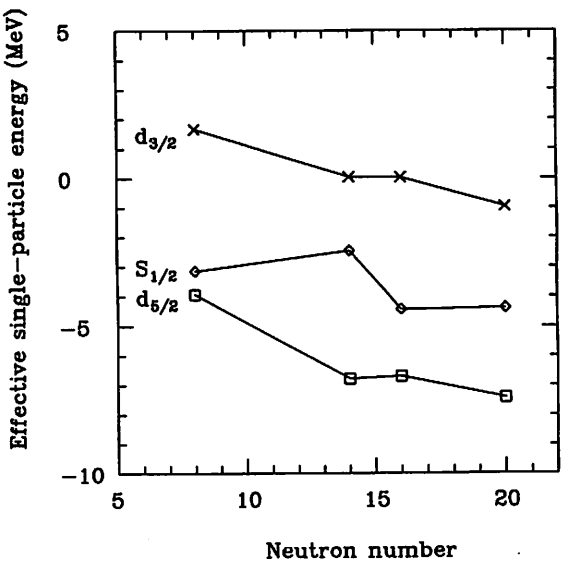

FIGURE 2. Neutron single-particle energies as a function of N.

of neutron number in this j–j coupling limit. The neutron ESPE are seen to be rather constant as a function of neutron number. This leads to a simple qualitative interpretation for the binding energy curve shown in Fig. 1. Between $N = 8$ and 14 the neutrons fill the $d_{5/2}$ orbit which is bound in ^{16}O by about 4 MeV. This, together with the attractive pairing energy, provides the sharp increase in binding energy observed between $N = 8$ and 14. Between $N = 14$ and 16 the neutrons fill the $s_{1/2}$ orbit which is less bound than the $d_{5/2}$. Thus one starts to see less increase in the binding energy at this point. Between $N = 16$ and 20 the neutrons fill the $d_{3/2}$ orbit which has close to zero energy, and the binding energy curve becomes flat in this region. This flatness, of course, makes it difficult to predict exactly which nuclei will be stable. Beyond $N = 20$ the neutrons must start to go into the pf shell orbits which are unbound. Hence the binding energy curve decreases beyond this point. This marks the end of where the $Z = 8$ isotopes can be studied and also the end of where they need to be understood for astrophysical purposes.

At the next level of detail one should take into account the small shifts in the neutron ESPE shown in Fig. 2. These are again due to the interactions within the shells. For example the shift in the $s_{1/2}$ ESPE between ^{16}0 and ^{22}O is due the monopole average over two-body matrix elements:

$$\frac{\sum_J (2J+1)\langle d_{5/2}, s_{1/2}, J|V|d_{5/2}, s_{1/2}, J\rangle}{\sum_J (2J+1)}.$$

It is important to note that these two-body matrix elements can in principle be obtained from information on excited states in ^{18}O and ^{19}O etc. Data on excitation energies relevant to these $d_{5/2}$–$s_{1/2}$ two-body matrix elements were included in the 447 fit-data set used

to obtained the W and SDPOTA interactions. Hence, the good agreement for the ^{23}O and ^{24}O mass predictions may not be surprising even though data on these two nuclei were not included in the fit-data set. In contrast, beyond ^{24}O, the ESPE depend on the $d_{5/2}$–$d_{3/2}$ two-body matrix elements. Data on excitation energies relevant to these do not exist because they are more highly excited configurations and lie in a large level density of intruder states. Hence beyond ^{24}O, the predictions rely more on assumptions in the calculation which cannot be tested from previously known data. For the W interaction the Kuo-Brown G matrix was used for the poorly determined linear combinations, and for the SDPOTA interaction the fitted potential model was used (a modified surface one-boson exchange potential).

The actual *sd*–shell calculations shown in Fig. 1 go beyond *j*–*j* coupling and include all possible *sd*–shell configurations. But again, the dominant configurations are those assumed above. These calculations, it should be remembered, are based on zeroth-order perturbation theory together with an assumed constancy of the bare SPE and an assumed simple $(A/18)^{0.3}$ mass dependence of the two-body matrix elements [8,16]. Presumably nature is more complicated than this. But, given the continued success of the shell-model in correlating all observed data, these complications must get folded into the effective nature of the interactions in a way that may never be fully quantitatively understood. The next major step in the *sd*–shell calculations will be to incorporate all of the new data which has appeared since the original fit-data set was put together about ten years ago [16].

The differences between experimental and theoretical (W) binding energies for all nuclei between $Z = 8$–20 are shown in Fig. 2 of Ref. [11]. The predictions are based on W–*sd* for $N \leq 20$ and WBMB *sd*–*pf* for $N > 20$. The agreement between experiment and theory is good for most cases. There are some exceptional deviations. For $N = 18$ and $9 \leq Z \leq 13$ there is a pronounced glitch which may be due to a similar kind of model-dependence left in the W interaction as discussed above for ^{26}O. The more dramatic deviations in the most neutron rich Na and Mg isotopes, which have been known for many years [24], point to the intruder state problem which is discussed in the next section.

3. CROSS-SHELL EXCITATIONS AROUND ^{32}MG

The anomalies in the binding energies, excitation energies, half-lives and radii of the most neutron rich Na and Mg isotopes relative to the type of $0\hbar\omega$ calculations described above have been known for a long time [24]. The situation has been referred to as the "collapse of the conventional shell model" [25]. Several studies over the past ten years have indicated that the problem is due to low-lying intruder states from the pf shell [26,27,28]. I summarize here the results of a new set of systematic calculations with the WBMB interaction for these intruder states [11]. These new calculations incorporate all of the sd and pf orbits and represent the most ambitious calculations to date. An advantage (and disadvantage) of our calculations is that there are no adjustable parameters. The WBMB cross-shell interaction [11] was obtained from a fit of the Millener-Kurath potential model [20] parameters and some fine tuning of some individual two-body matrix to reproduce the excitation energies of $1p$–$1h$ states in ^{40}Ca and ^{40}K.

An important aspect of our calculations is that we do not allow for explicit mixing between $0\hbar\omega$, $2\hbar\omega$, $4\hbar\omega$, etc. configurations or between $1\hbar\omega$, $3\hbar\omega$ etc. configurations. The rationale for this restriction is related to the "excitation-order" problem discussed in Ref. [8] and is discussed more in the present context in Ref. [11]. The standard shell-model interactions one is familiar with, such as the W–*sd* interaction, are designed to reproduce binding energies without such explicit mixing and must already incorporate this mixing implicitly. Our experience with the well-known $n\hbar\omega$ intruder states near ^{16}O and ^{40}Ca indicates that these different excitations tend to "coexist" rather than to strongly mix with each other. Our point of view is that we do not at present know how to deal with explicit mixing and that hopefully "coexistence" will continue to hold.

This is one of the major differences between our calculations and those of Poves and Retamosa [27] and Fukunishi *et al.* [12], where explicit mixing between major shells is allowed. Poves and Retamosa mix an extremely deformed $2\hbar\omega$ ground state band (e.g. with the 2^+ energy around 200 keV) with the normal $0\hbar\omega$ states to get resulting spectra which are moderately deformed (e.g. with the 2^+ energy around 800 keV). Our calculation, with no mixing, and the Poves-Retamosa calculation, with large mixing, give qualitatively the same spectra.

Full space $1\hbar\omega$ and $2\hbar\omega$ *sd–pf* calculations are possible for ^{28}O, ^{29}F and ^{30}Ne. From these studies we determined that the proton excitations from sd to pf could safely be ignored. The important configuration was found to correspond to a $2\hbar\omega$ neutron excitation. This configuration had an excitation energy relative to the lowest $0\hbar\omega$ state in these three nuclei of 2.96 MeV, 1.34 MeV, and −0.79 MeV, respectively. The full-space calculations for most of the nuclei of interest around ^{32}Mg have dimensions which are too large to handle. We investigated several truncations which have promise for future calculations. However, the most interesting and useful result found in these investigations is that a weak-coupling model can be used to relate the excitation energy of the $n\hbar\omega$ configurations to the calculated $0\hbar\omega$ binding energies in nuclei with neighboring neutron numbers. Many examples, of the weak-coupling model have been discussed for nuclei around ^{16}O and ^{40}Ca where the residual interaction between particles and holes has an isospin-dependence [29,30]. In our case the form of the particle-hole interaction is much simpler since only neutrons are excited.

With the weak coupling approximation we have been able to calculate excitation energies for the 1, 2 and $3\hbar\omega$ configurations for nuclei near ^{32}Mg. The surprising result is that there is an island of nuclei in which the $2\hbar\omega$ configuration comes lower in energy that the $0\hbar\omega$ configuration, namely $^{32-34}$Mg, $^{31-33}$Na and $^{30-32}$Ne, and there are many others for which the $1\hbar\omega$ configuration is essentially degenerate with the $0\hbar\omega$ configuration analogous to the famous $1/2^-$, $1/2^+$ doublet in ^{11}Be. The additional binding energy associated with these "intruder" configuration explains much of the discrepancy seen between experiment and the $0\hbar\omega$ calculations. (Also see the comparison to more recent experimental data given by Orr *et al.* [31].)

We find that there are three mechanisms which combine to give the inversion of $2\hbar\omega$ relative to $0\hbar\omega$: the (small) reduction in the ESPE gap, the pairing energy E_{nn}, and the proton-neutron interaction energy E_{pn}. The only one of which should have a strong Z dependence is E_{pn}.

For all $N = Z$ nuclei in the sd shell, there are low-lying (1.4–2.2 MeV) collective 2^+ states. When both protons and neutrons fill the beginning of a major shell there are strong ^{4}He-type correlations which lead to well-defined prolate deformations as in the case of ^{20}Ne and ^{24}Mg in the sd shell. The prolateness of ^{20}Ne and ^{24}Mg is reinforced by the small energy gap between the $d_{5/2}$ and $s_{1/2}$ orbits in the lower part of the *sd* shell. In $N = Z$ nuclei in the middle to end of a major shell there is a competition between prolate and oblate deformations as in the case of ^{28}Si, ^{32}S and ^{36}Ar in the *sd* shell. For these nuclei the type of collectivity is particularly sensitive to the spacing of the single-particle orbits in the major shell.

It is well known that $n\hbar\omega$ configurations often lie very low in excitation energy for the reasons discussed above. The lowing lying $4\hbar\omega$ 4p-4h configuration in ^{16}O and its explanation in terms of a weak-coupling model [29,30] is perhaps the most famous example. But by the time we reach $A = 80$ the nominal shell closure of the *pf* shell is lost by the lowering of the $g_{9/2}$ orbit, and beyond this point it is well known that magic numbers are no longer those of the major harmonic oscillator shells. The mechanisms behind our island of inversion are also responsible for the low-lying intruder states in heavy nuclei [32]. This suggests obvious applications of the weak-coupling approximation to these heavy nuclei. Relationships to the deformed shell-model approach have also been pointed out [33]. In addition, we note that there is a similar intruder state problem in the region around ^{12}Be, where the ground state of ^{11}Be has a well-known $1\hbar\omega$ $1/2^+$ configuration. The intruder state problem in this region is currently being studied in a model which takes into account the mixing between $n\hbar\omega$ configurations [34].

ACKNOWLEDGEMENTS

This work was supported by the US National Science Foundation grant number PHY-90-17077.

REFERENCES

1. B.A. Brown, *Phys. Rev. Lett.* **69** (1992) 1034.
2. B.A. Brown, *Phys. Rev. Lett.* **65** (1990) 2753.
3. B.A. Brown, *Phys. Rev.* **C43** (1991) 1513; **C44** (1991) 924.
4. B.A. Brown, A. Arima and J.B. McGrory, *Nucl. Phys.* **A277** (1977) 77.
5. H. Kitagawa and H. Sagawa, *Phys. Lett.* **B299** (1993) 1.
6. H. Esbensen and G.F. Bertsch, *Phys. Rev.* **C46** (1992) 1552; *Nucl. Phys.* **A542** (1992) 310.
7. G.F. Bertsch, B.A. Brown and H. Sagawa, *Phys. Rev.* **C39** (1989) 1154; H. Sagawa, *Phys. Lett.* **B286** (1992) 7.
8. B.A. Brown and B.H. Wildenthal, *Ann. Rev. of Nucl. and Part. Sci.* **38** (1988) 29.
9. W.D.M. Rae, A. Etchegoyen and B.A. Brown, MSU Cyclotron Laboratory Report No. 524.
10. B.A. Brown, *Workshop on Microscopic Models in Nuclear Structure Physics*, World Scientific (1989) pp. 337–355.
11. E.K. Warburton, J.A. Becker, and B.A. Brown, *Phys. Rev.* **C41** (1990) 1147.
12. N. Fukunishi, T. Otsuka and T. Sebe, *Phys. Lett.* **B**, in print.
13. N. Nakada, T. Otsuka and T. Sebe, *Phys. Rev. Lett.* **67** (1991) 1086.
14. S. Cohen and D. Kurath, *Nucl. Phys.* **73** (1965) 1, *Nucl. Phys.* **A101** (1967) 1.

15. E.K. Warburton and B.A. Brown, *Phys. Rev.* **C46** (1992) 923.
16. B.H. Wildenthal, *Progress in Particle and Nuclear Physics* **11**, edited by D.H. Wilkinson, Pergamon, Oxford (1984) p. 5.
17. B.A. Brown, W.A. Richter, R.E. Julies and B.H. Wildenthal, *Ann. Phys.* **182** (1988) 191.
18. J.B. McGrory, *Phys. Rev.* **C8** (1973) 693.
19. W.A. Richter, M.G. Van der Merwe, R.E. Julies and B.A. Brown, *Nucl. Phys.* **A523** (1991) 325.
20. D.J. Millener and D. Kurath, *Nucl. Phys.* **A255** (1975) 315.
21. D. Guillemaud-Mueller *et al., Phys. Rev.* **C41** (1990) 937.
22. P. Moeller and J.J. Nix, *At. Data Nucl. Data Tables* **39** (1988) 231.
23. A.H. Wapstra, G. Audi and R. Hoekstra, *At. Data Nucl. Data Tables* **39** (1988) 281.
24. C. Thibault *et al., Phys. Rev.* **C12** (1975) 644; C. Detraz *et al., Nucl. Phys.* **A394** (1983) 378; C. Detraz *et al., Phys. Rev.* **C19** (1979) 164.
25. B.H. Wildenthal and W. Chung, *Phys. Rev.* **C19** (1979) 164.
26. X. Campi *et al., Nucl. Phys.* **A251** (1975) 193.
27. A. Poves and J. Retamosa, *Phys. Lett.* **B184** (1987) 311.
28. M.H. Storm, A. Watt and R.R. Whitehead, *J. Phys.* **G9** (1983) L165; A. Watt, R.P. Singhal, M.H. Storm and R.R. Whitehead, *J. Phys.* **G7** (1981) L145.
29. L. Zamick, *Phys. Lett.* **19** (1965) 580.
30. R.D. Lawson, *Theory of the Nuclear Shell Model*, Clarendon Press, Oxford (1980).
31. N.A. Orr, *Phys. Lett.* **B258** (1991) 29.
32. K. Heyde *et al., Physics Reports* **102** (1983) 291; *Phys. Rev.* **C38** (1984) 984; *Nucl. Phys.* **A466** (1987) 189; *Nucl. Phys.* **A484** (1988) 275.
33. K. Heyde *et al., Phys. Lett.* **218B** (1989) 298.
34. E.K. Warburton, B.A. Brown and D.J. Millener, *Phys. Lett.* **B293** (1992) 7.